



SCAPER localizes to primary cilia and its mutation affects cilia length, causing Bardet-Biedl syndrome

Ohad Wormser¹ · Libe Gradstein² · Yuval Yogev¹ · Yonatan Perez¹ · Rotem Kadir¹ · Inna Goliand³ · Yair Sadka⁴ · Saad El Riati⁵ · Hagit Flusser⁶ · Dikla Nachmias³ · Ruth Birk⁷ · Muhamad Iraqi¹ · Einat Kadar¹ · Roni Gat³ · Max Drabkin¹ · Daniel Halperin¹ · Amir Horev⁸ · Sara Sivan¹ · Uri Abdu⁹ · Natalie Elia³ · Ohad S. Birk^{1,10}

Received: 3 May 2018 / Revised: 17 December 2018 / Accepted: 4 January 2019 / Published online: 5 February 2019
© European Society of Human Genetics 2019

Abstract

Studies of ciliopathies have served in elucidating much of our knowledge of structure and function of primary cilia. We report humans with Bardet-Biedl syndrome who display intellectual disability, retinitis pigmentosa, obesity, short stature and brachydactyly, stemming from a homozygous truncation mutation in *SCAPER*, a gene previously associated with mitotic progression. Our findings, based on linkage analysis and exome sequencing studies of two remotely related large consanguineous families, are in line with recent reports of *SCAPER* variants associated with intellectual disability and retinitis pigmentosa. Using immuno-fluorescence and live cell imaging in NIH/3T3 fibroblasts and SH-SY5Y neuroblastoma cell lines over-expressing *SCAPER*, we demonstrate that both wild type and mutant *SCAPER* are expressed in primary cilia and co-localize with tubulin, forming bundles of microtubules. While wild type *SCAPER* was rarely localized along the ciliary axoneme and basal body, the aberrant protein remained sequestered to the cilia, mostly at the ciliary tip. Notably, longer cilia were demonstrated both in human affected fibroblasts compared to controls, as well as in NIH/3T3 cells transfected with mutant versus wildtype *SCAPER*. As *SCAPER* expression is known to peak at late G1 and S phase, overlapping the timing of ciliary resorption, our data suggest a possible role of *SCAPER* in ciliary dynamics and disassembly, also affecting microtubule-related mitotic progression. Thus, we outline a human ciliopathy syndrome and demonstrate that it is caused by a mutation in *SCAPER*, affecting primary cilia.

Supplementary information The online version of this article (<https://doi.org/10.1038/s41431-019-0347-z>) contains supplementary material, which is available to authorized users.

✉ Ohad S. Birk
obirk@bgu.ac.il

- ¹ The Morris Kahn Laboratory of Human Genetics, National Institute for Biotechnology in the Negev and Faculty of Health Sciences, Ben-Gurion University of the Negev, 84105 Beer Sheva, Israel
- ² Department of Ophthalmology, Soroka Medical Center and Clalit Health Services, Faculty of Health Sciences, Ben-Gurion University, 84101 Beer Sheva, Israel
- ³ Department of Life Sciences and National Institute for Biotechnology in the Negev, Ben Gurion University of the Negev, 84105 Beer Sheva, Israel
- ⁴ Child Developmental Center, Beer Sheva Mental Health Center, Ben-Gurion University of the Negev, 84101 Beer Sheva, Israel

Introduction

Diseases of ciliary function (ciliopathies) affect motile cilia, immotile cilia, or both of these microtubule-based structures [1]. The immotile primary cilium functions as a cellular

- ⁵ Clalit Health Services, Southern district, P.O. Box 616, 30 Itzhak Rager Street, Beer sheva, Israel
- ⁶ The Zusman Institute for Child Development, Division of Pediatrics, Soroka Medical Center and Ben-Gurion University of the Negev, 84101 Beer Sheva, Israel
- ⁷ Department of Nutrition, Faculty of Health Sciences, Ariel University, Ariel, Israel
- ⁸ Department of Dermatology and Venereology and Division of Pediatrics, Soroka Medical Center and Faculty of Health Sciences, Ben-Gurion University of the Negev, 84101 Beer Sheva, Israel
- ⁹ Department of Life Sciences, Ben-Gurion University, 84105 Beer Sheva, Israel
- ¹⁰ Genetics Institute, Soroka Medical Center, Ben-Gurion University of the Negev, 84101 Beer Sheva, Israel

sensor for mechanical and chemical environmental cues, and is subjected to dynamic regulation during cell cycle progression [2]. Gaps remain in understanding ciliopathies and the proteins involved, and new core or regulatory players are yet to be identified [1]. Ciliopathies described to date include, among others, polycystic kidney disease, Meckel-Gruber syndrome, Joubert syndrome, Nephronophthisis, Alstrom syndrome, and Bardet-Biedl syndrome (BBS) [1]. BBS is phenotypically heterogeneous [3–5] and exhibits genetic heterogeneity, with 21 BBS genes known to date and others yet to be identified [6–9]. The Bedouin community of southern Israel, in which several BBS mutations have been discovered [6], has high rates of consanguinity culminating in many inherited diseases arising from founder mutations [10, 11]. High prevalence of BBS among this cohort (1:13,500) has been noted, compared to 1:1,60,000 in north Europeans [4, 12]. We now describe a consanguineous Bedouin kindred with multiple individuals affected by BBS, and demonstrate that the disease is caused by a mutation in *SCAPER*, localized in cell culture to primary cilia.

Materials and methods

The study was approved by the Soroka Medical Center institutional review board (approval #5071G). DNA samples, RNA samples and skin punch biopsies were obtained following written informed consent. Detailed methods are given in Supplementary Materials and Methods.

Linkage analysis

Genome-wide linkage analysis was performed using Illumina Omni Express Beadchip with >700 K SNP loci per sample (Illumina, San Diego, CA, USA), as previously described [13]. Homozygosity mapping analysis was carried out using Homozygosity-Mapper [14], and Multipoint Logarithm of Odds (LOD) score for the pedigree P1 (Fig. 1a) was calculated via SUPERLINK ONLINE SNP 1.1 [15]. Copy number variations (CNVs) were analyzed using microarrays' log *R* ratio (PARTEK®).

Sequence analysis

Whole exome sequencing (WES) of DNA samples of individuals P1:V6 and P1:V7 (Fig. 1a) was performed as previously described [13, 16] at a mean coverage of 30-fold and 68.8-fold, respectively; accordingly, 85% and 97.5% of all exonic nucleotides and splice junctions were covered by >10 reads. Sequences with low reads (<5×) in the WES data within the disease-associated chromosome 15 locus (Fig. 1b) were re-sequenced by Sanger sequencing. The

SCAPER variant was further assayed through restriction fragment length polymorphism (RFLP) using *Nla*IV endonuclease analysis and multiple sequence alignment (further expanded in Supplementary Materials and Methods).

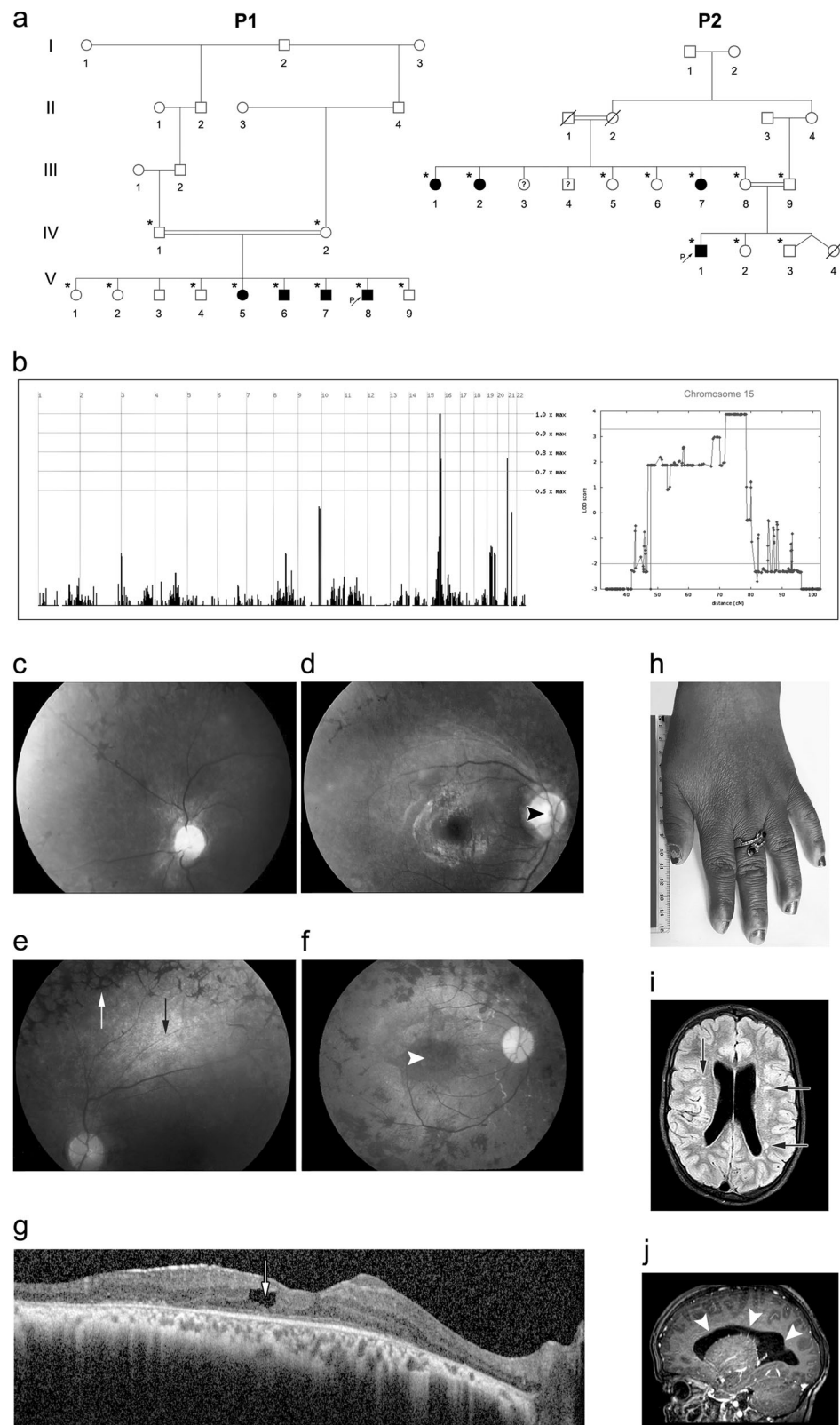
Quantitative reverse transcription PCR

RNA was extracted from fresh peripheral blood leukocytes of patients P2:IV1, P2:III1, and P2:III2 (Fig. 1a). PCR primers were designed to amplify cDNA rather than genomic DNA of human *SCAPER* and of glyceraldehyde 3-phosphate dehydrogenase (*GAPDH*) housekeeping gene as a control. After amplification, sequences were validated through Sanger sequencing.

Plasmid constructs

Plasmid pCBF-FLAG-SCAPER, harboring the *SCAPER* long isoform driven by a CMV promoter, was a kind gift of William Tsang (Institut de recherches cliniques de Montréal; IRCM) [17, 18]. In-vitro mutagenesis, inserting the human *SCAPER* mutation (c.2806delC; p.(L936*), NM_020843.2), was done using primers 5'-GATCGGA CCTAGGAGAGAT-3' and 5'-CTCTCCTAGGTCCGAT CCAA-3', and Q5® High-Fidelity DNA polymerase, creating the pCBF-FLAG-mutSCAPER. Mock pCBF plasmid (pCBF-FLAG) was produced by restriction using *Nsi*I and *Eco*RV (cutting out the entire *SCAPER* gene from pCBF-FLAG-SCAPER), following blunting and ligation, expressing only FLAG followed by 20 amino acids until reading-frame termination. Sequences of the wild type (WT) and mutated plasmids were validated by Sanger sequencing. *SCAPER* cDNA was next sub-cloned to C1-mCherry plasmids from pCBF-FLAG-SCAPER, and pCBF-FLAG-mutSCAPER (c.2806delC; p.(L936*)), using restriction endonucleases *Xho*I and *Eco*RV, following blunting and ligation. Plasmids C1 mCherry-WT-SCAPER, C1 mCherry-MUT-SCAPER and C1 mCherry (mCherry-mock) sequences were validated using restriction endonucleases and through Sanger sequencing for having *SCAPER* long isoform, N' tagged with mCherry with a linker of 6 amino acids, driven by CMV promoter. Next, *SCAPER* cDNA was subcloned to mEGFP-C1 (EGFP with p.(A206K) substitution), using restriction endonucleases *Bsp*EI and *Acc*65I for mEGFP-C1, and *Sgr*AI and *Acc*65I for the mCherry-SCAPER WT and MUT plasmids, creating mEGFP-WT-SCAPER, and mEGFP-MUT-SCAPER. The constructs were validated using restriction endonucleases and Sanger sequencing for having long isoform of *SCAPER* (WT or MUT), preceded by a mEGFP and linker of 9 amino acids. N' tagging of *SCAPER* was preferred, as a C' terminus ER-retrieval signal may be essential [17]. Plasmid GFP- α -tubulin, containing the full-length human α -tubulin

Fig. 1 Pedigree, homozygosity mapping and disease phenotype: **a** Pedigrees of consanguineous Bedouin kindred studied (P1—pedigree 1, P2—pedigree 2). Subjects available to the study are marked with asterisks. All eight affected individuals were homozygous for the *SCAPER* (NM_020843.2) c.2806delC; p.(L936*) mutation. **b** Homozygosity-Mapper plot and LOD score analysis for chromosome 15 using SUPERLINK online. **c–e** Fundus photographs of three P1 patients: **c** P1:V7 (14 years) (left eye), **d** P1:V6 (27 years) (right eye), **e** P1:V5 (33 years) (left eye), showing diffuse chorio-retinal degeneration, as evidenced by attenuated arterioles (black arrow), granular appearance of the retina with hypopigmented spots, optic disk pallor (black arrowhead) and a typical bone-spicule type hyperpigmentation (white arrow) in the retinal mid-periphery. **f** Fundus photograph of the right eye of patient P2:III2 (47 years), showing optic atrophy, attenuated vessels, gray atrophic retina with diffuse coarse pigment clumps and bone spicules, as well as a severe maculopathy (white arrowhead) seen also on the SD-OCT image of this eye. **g** Irregular and thickened foveal margins and intra-retinal fluid with cystoid macular edema (arrow) (patient P2:III2). **h** Brachydactyly with tapering fingers (patient P2:III1). **i, j** Brain MRI of patient P2:IV1 at the age of 10 years, demonstrating mildly enlarged lateral ventricles (**i**; arrows) and several loci of irregular signal in the brain parenchyma (**j**; arrowheads) above the tentorium, in the posterior white matter and along the ependyma



cloned into pEGFP-C1 was used as previously described [19].

Cell culture and transfection

HeLa, SH-SY5Y and primary fibroblasts were grown in standard media. NIH/3T3 cells were grown in low glucose (1 g/L D-Glucose) DMEM with sodium pyruvate, supplemented with 10% newborn calf serum, 2 mM glutamine, 10,000 U/ml penicillin, and 10 mg/mL streptomycin. Transfections were carried out using linearized polyethylenimine (PEI; Polysciences Inc., USA) or Lipofectamine® 2000 (Thermo Fisher Scientific, USA), employing standard techniques. A 4-mm human skin punch biopsy was dissected and prepared for derivation of fibroblast culture, following standard methods [20].

Western blot analysis

HeLa cells were plated in 12-well plates and transfected using PEI with plasmid DNA: pCBF-FLAG-SCAPER, pCBF-MOCK, or p.(L936*) pCBF-FLAG-mutSCAPER. Thirty-six to 48 h after PEI transfection, cells were harvested and total protein samples were resolved on 7% SDS-polyacrylamide gel electrophoresis and subjected to western blot analysis.

Immunostaining and live cell imaging

For immuno-staining of ciliated cells, low passage NIH/3T3 were seeded on coverslips in 12-well plates, and transfected the following day (at 40–60% confluence) with mCherry-WT-SCAPER, mCherry-MUT-SCAPER, C1-mCherry (mCherry-mock), mEGFP-WT-SCAPER, mEGFP-MUT-SCAPER or C1-mEGFP (mEGFP-mock). For live-cell imaging, cells were directly seeded on 4 wells μ -slides (ibidi GmbH, Germany) and transfected in wells the following day with one of the following: mEGFP-WT-SCAPER, mEGFP-MUT-SCAPER, C1-mEGFP (without further fixation and immunostaining); or with one of the following: mCherry-WT-SCAPER, mCherry-MUT-SCAPER, mCherry-mock, co-transfected with GFP- α -tubulin. Sixteen to thirty hours following transfection, cells were washed, fixed, stained, mounted and visualized using LSM880 microscope with 20 \times /0.8 and 60 \times /1.4 objectives (Carl Zeiss Microscopy GmbH, Germany). Primary cilia were immuno-stained using primary antibodies which mark the axoneme and adjacent basal body: for the axoneme, anti acetylated alpha tubulin antibody (ab24610, mouse monoclonal Ab to acetylated alpha tubulin [6-11B-1], Abcam, UK); for the basal body, anti-gamma tubulin antibody (ab11317, rabbit polyclonal to gamma tubulin, Abcam, UK). Both were used as primary antibodies alone or together. For live cell

imaging and mEGFP plasmids-transfected cells, Fast-Airy-Scan mode in LSM880 was used. Same lenses and parameters (such as master gain, digital gain, digital offset, and pinhole size) were used in all experiments (and within Airy-Scan experiments separately), after ensuring there was no leakage of emitted light between the 3 or 4 different fluorophores used in all experiments. All pictures represent maximum intensity projection of all planes (about 9–14 for each field, and 18–25 for the live cells), generated using ZEN 2.3 (Carl Zeiss Microscopy GmbH, Germany). Fields were selected randomly and counted manually. Only cells having one easily defined protruding cilium, preferably marked with anti-gamma-tubulin on one end, were counted as ciliated. Of note: in Fig. 3c–e represent transfections with both mCherry and mEGFP conjugated fluorophores, and at least 4 biological replicates of those cells, fixed 24 h post transfection, grown and transfected at similar conditions. *p* value was calculated from observed (counted) vs predicted tables using χ^2 test between each two populations for panels c and d, and *t*-test (2 tails, unequal variance) for panels e and f. In graphs e and f, cilia measurements were calculated with ZEN 2.3 (Carl Zeiss Microscopy GmbH, Germany), using only photos taken with a 60 \times /1.4 objective.

Primary fibroblasts and scanning electron microscope (SEM)

Cells derived from an affected patient (P2:IV1) and an age and ethnicity-matched control individual, at a similar passage, were seeded on coverslips and grown to confluency. After additional 48 h serum-starvation, cells were washed, fixed, stained, mounted and visualized using LSM880 microscope with 60 \times /1.4 objectives as previously described (for confocal microscopy), or fixed with warm glutaraldehyde, treated with Osmium tetroxide, critical-point dried and gold-coated, before observing using SEM (further elaborated in the supplementary methods). For cilia length quantification, maximum intensity projections of 40 images, representing large fields randomly selected from three different experiments (technical replicates), were analyzed using ZEN 2.3 (Carl Zeiss Microscopy GmbH, Germany).

Results

Delineation of the disease phenotype

Twenty individuals, of two consanguineous Bedouin families of the same tribe in southern Israel, were recruited for this study (Fig. 1a). The clinical phenotype is delineated in Fig. 1; Table 1: all eight affected individuals (ages 10–48 years) exhibited developmental delay/intellectual disability, with severe speech delay, speaking only few words beyond

Table 1 Patients' phenotypes (Human Phenotype Ontology nomenclature)

Patient ID	P1:V5	P1:V6	P1:V7	P1:V8	P2:III1	P2:III2	P2:III7	P2:IV1
Patient age (years)/sex	34/F	28/M	24/M	17/M	48/F	47/F	29/F	10/M
Retinitis pigmentosa HP:0000580	+	+	+	+	+	+	+	Suspected
Intellectual disability HP:0010864I ^a	Moderate	Moderate	Moderate	Moderate	Severe	Severe	Severe	Moderate
Short stature HP:0004322 (height, cm OR percentile)	+(145)	+(157)	+(163)	+(155)	+(146)	+(149)	+(132)	Percentile 3–5% (129)
Weight (kg)	78	78	98	92	86.6	62	57.8	29.5 (percentile 25–50%)
Obesity HP:0001513 (calculated BMI kg/m ²)	+(37.1)	+(31.6)	+(36.9)	+(38.3)	+(40.6)	-Overweight (27.9)	+(33.2)	BMI-for-age at the 68th percentile ^b
Genu Valgum HP:0002857/Genu Varum HP:0002970	+	+	+	+	?	+	?	+
Speech Delay HP:0002167	+	+	+	+	+	+	+	+
Brachydactyly HP:0001156	+	+	+	+	+	+	+	+

^aA formal IQ test could not be done due to low compliance. We have estimated the level of ID based on basic daily skills and the intensity of support needed either observed or when not available for clinical appreciation—based on medical records (as DSM V assesses the level of severity based on adaptive functioning and not IQ score)

^bAccording to the Centers for Disease Control and Prevention (CDC)—BMI percentile calculator for child and teen

10 years of age. All adult patients had short stature and obesity (apart from one patient that was overweight—BMI 28). Brachydactyly with tapering fingers were evident in all of the patients, and six had genu valgum or varum (Fig. 1h). None of the patients had microcephaly or facial dysmorphism. Four patients exhibited inappropriate behavior (mental confusion, inappropriate affect, inability to comply with simple instructions). Three patients had unstable gait and two of them were wheelchair-ridden. None had clinical evidence of polydactyly, diabetes, anosmia, hypogonadism, or kidney abnormalities (per ultrasound and blood creatinine levels). Seven of the affected individuals, 17 years of age or older, were diagnosed with severe retinitis pigmentosa (RP), with initial evidence of RP in the youngest (10 years old) patient (Table 1 and S1 Table). In both families, progressive loss of night vision began in the first or second decade of life, followed by difficulties in daytime vision as well. Visual acuity ranged from 6/10 in the youngest patient to only light perception in the oldest (Table 1 and Table S1). Affected individuals older than 30 years of age had severe visual handicap and were not able to ambulate without assistance. Four patients had strabismus (exotropia). Refractive errors included mild myopia and astigmatism. In five older patients, cataract was demonstrated (posterior sub-capsular in most). Fundoscopy revealed bone-corporuscular pigmentation typical of RP in all but one patient (Fig. 1c–f). In three of the older patients, optic atrophy, narrow retinal vessels and gray retinal discoloration were also detected. Two patients of Pedigree 2 had also severe maculopathy as demonstrated by fundus photography and spectral domain optical coherence tomography

(SD-OCT) imaging of the retina of patient P2:III2 (Fig. 1f, g). Electroretinography (ERG), performed on two patients (P1:V5 and P1:V6) aged 25 and 17 years, showed extinguished retinal responses from both eyes at dark-adapted and light-adapted conditions, even with higher than standard light stimuli. Flash visual evoked potentials (VEP) testing of patient P1:V5 elicited increased-latency responses. In the youngest patient, P2:IV1, age 10 years, it was technically impossible to assess vision; his fundus exam showed mild optic disk pallor and gray retinal discoloration, suggesting possible retinal dystrophy.

Aside from the phenotypes shared by all or most patients, single patients had additional unique findings—not necessarily related to the familial syndrome: one patient in family P1 also suffered from epilepsy and facial nerve palsy and one had congenital heart defects (tetralogy of Fallot). Attention deficit hyperactivity disorder (ADHD) was diagnosed in an affected individual in family P2. Brain computed tomography (CT) of this patient (P2:IV1) at the age of 8 months showed enlarged 3rd and 4th ventricles, rounding of sub-arachnoid spaces and borderline white matter abnormality; more recent magnetic resonance imaging (MRI) (age 10 years) revealed mild enlarged lateral ventricles and several loci of irregular signal in the brain parenchyma above the tentorium, in the posterior white matter and along the ependyma (Fig. 1i, j).

Identification of the SCAPER mutation

Patients' karyotypes and chromosomal microarray analyses were normal (data not shown). Analysis of whole-exome

sequencing (WES) data of individuals P1:V6 and P1:V7 identified no mutations in known ciliopathy-related genes, including all BBS genes. Genome-wide homozygosity mapping, analyzing single nucleotide polymorphism (SNP) data of all available subjects in family P1, identified a single homozygosity segment shared exclusively by all affected individuals (Fig. 1b). This chromosome 15 locus (between SNPs rs8040073 and rs4886566, positioned respectively at 70,760,574 and 78,563,652 in the GRCh37/Hg19 assembly) segregated within the kindred as expected for autosomal recessive heredity. Maximal multipoint LOD score was 3.88 (Fig. 1b). Sanger sequencing was done for all exons and exon-intron boundaries within the locus whose coverage in the WES was insufficient (<5×). Notably, no sequence variations were found within *BBS4* (NM_033028.4) and *SIN3A* (NM_015477.2) within this locus—genes whose mutations are known to cause overlapping phenotypes [21, 22]. Five rare variants were found within this locus, in *UACA*, *THSD4*, *C15ORF39*, *TMEM266*, and *SCAPER*. Three of the variants (in *UACA*, *C15ORF39*, and *TMEM266*) were ruled out as being associated with the disease: the *UACA* (NM_001008224.2) c.3113T>C, p.(I1038T) (rs150879212) variant is a common polymorphism (4.375%) in our local Bedouin cohort of 160 ethnically-matched controls, and was previously identified in a homozygous state in an apparently healthy individual (reported in ExAC and gnomAD as not affected by severe pediatric disease; last accessed at 28th of July 2018, encompassing 123,136 exome sequences and 15,496 whole-genome sequences) [23–25]. The *TMEM266* (NM_152335.2) c.1343C>T, p.(S448L) (rs368038771) variant, with prevalence of 1.875% in our Bedouin cohort, represents a multi-allelic nucleotide, and is predicted to be a benign polymorphism (as the same amino acid substitution is common in some other mammals). The *C15ORF39* (NM_015492.4) variant c.610T>G, p.(S204A) (chr15:75498999), predicted to be a benign polymorphism by both PolyPhen-2 [26] and MutationTaster2 [27], with normal inferred activity in Ingnuity®, is the least conserved amino acid within the variants being studied, and is located in an area of relatively low WES coverage as seen in ExAC and gnomAD (the SNP was reported only in gnomAD database, at a low allele frequency of 0.003%, of 30,860 alleles sequenced (representing only whole genome sequencing data)). Thus, only two variants passed our filtration cascade and were predicted as possibly affecting function: *THSD4* (NM_001286429.1) c.1414G>A, p.(E472K) (chr15:72050319) missense variant, and *SCAPER* (NM_020843.2) c.2806delC; p.(L936*) (chr15:76866531) nonsense variant (Fig. 2a). The *SCAPER* variant was not found in our cohort or in allele frequency community (AFC), a freely accessible “opt-in” community resource designed to facilitate sharing of anonymized, pooled allele frequency statistics among laboratories, which already includes over

130,000 exomes/genomes; ca. May 2016, accessed at 12th of March 2017) [28]. Whereas the *THSD4* variant was more common (0.002% in AFC and 0.625% in our cohort) and multi-allelic, as another rare SNP (rs770207993; minor allele frequency 0.00003/4, ExAC) affects the same codon p.(E472G). Moreover, *THSD4* (also called *ADAMTSL6*) variants were previously related to aberrant pulmonary function and regulation of connective tissue [29, 30], not seen on our patients. Notably, mass spectrometry analysis of tissues, summarized in the ProteomicsDB database [31], originally from The Human Proteome Map (HPM) [32, 33], demonstrates that SCAPER protein is expressed in brain and retinal tissue, whereas there is no evidence of retinal expression of THSD4 (Fig. 2b). Thus, the *THSD4* variant is likely a polymorphism not associated with the disease phenotype. In contrast, the p.(L936*) (NM_020843.2) *SCAPER* variant is predicted to truncate the last third of the mature evolutionary-conserved protein (1400 amino acids) and to affect both validated transcripts of the mature mRNA (Fig. 2c). This transcript (named also ENST00000563290.5, translated to ENSP00000454973.1) appears as possibly cilia-related per the CilDB database [34] (database dedicated to proteins involved in centrioles, centrosomes, basal bodies, cilia and flagella in eukaryotes), as its homologs’ contributing peptides were detected in the centrosome proteome of *D. melangoster* [35], and in the cilium proteome (comprised of both cytoskeleton and photosensory-cilium) of *M. musculus* [36]. Furthermore, recent reports associated *SCAPER* sequence variants with autosomal-recessive intellectual disability, retinitis pigmentosa, ADHD and delayed motor development and cataracts, mostly in consanguineous families [37–40]. Thus, the disease phenotype likely stems from the *SCAPER* mutation.

Verification of mutations identified and population screening

Through RFLP (validated by Sanger sequencing) we demonstrated that the c.2806delC (NM_020843.2) *SCAPER* variant segregated within both affected families as expected for recessive heredity, with homozygosity in the eight affected individuals of families P1 and P2. Testing 325 individuals within the specific Bedouin tribe (225 of whom were specifically of the same clan of the affected families, predicted to demonstrate high similarity of prevalence of SNPs found, as it is a closed community), we could not rule-out either of the *THSD4*, *C15ORF39* and *SCAPER* variants, as they reside within the same haplotype, found as a homozygous stretch (between SNPs rs8040073 and rs4886566) only in the affected individuals. In all Bedouin controls tested, we found 2.8% heterozygous carriers of the *SCAPER* variant. It is noteworthy, that in highly inbred populations it is quite common to see 2.8% (and even more)

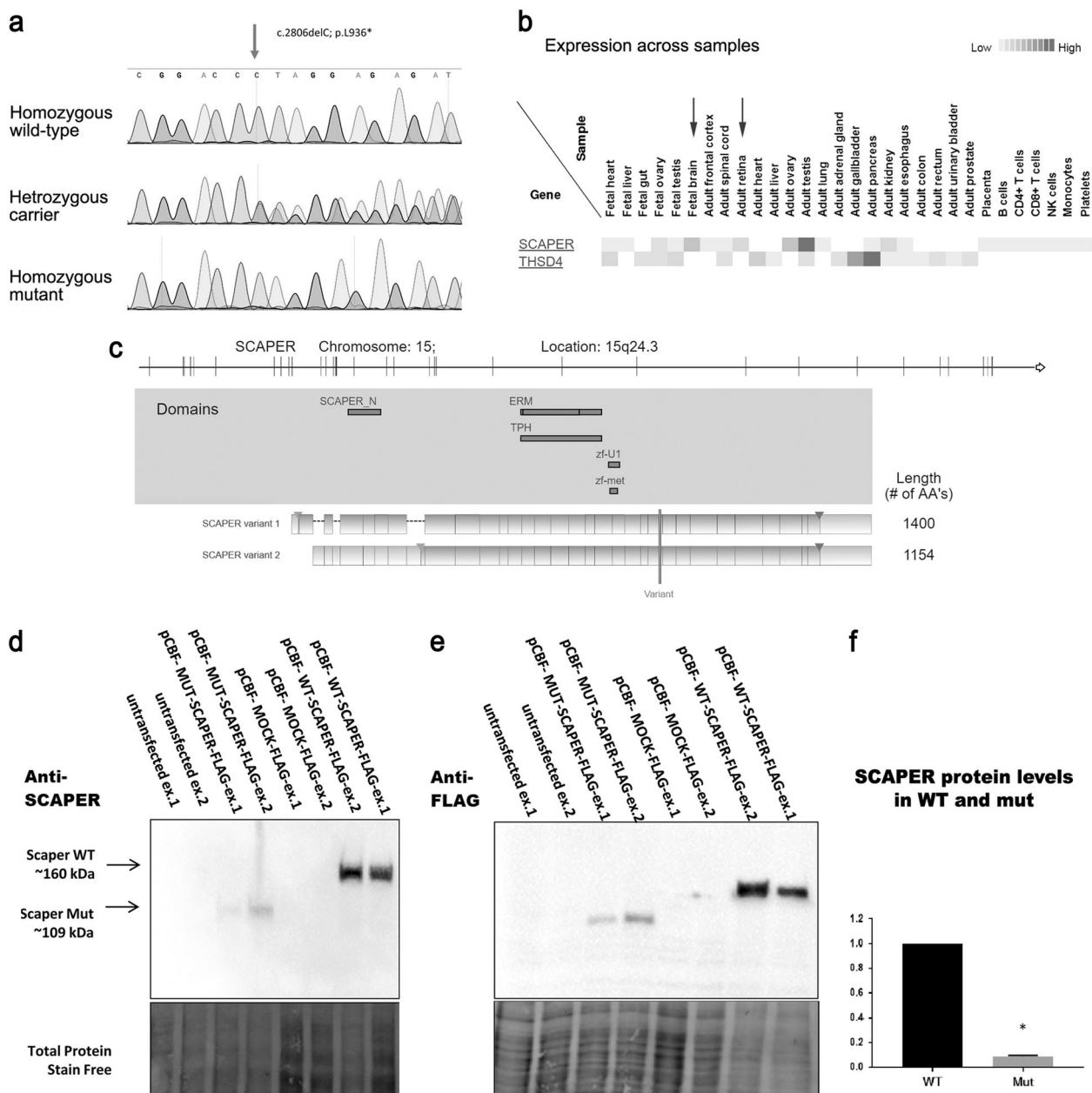


Fig. 2 *SCAPER* mutation, expression and conservation: **a** Sanger sequencing demonstrating the *SCAPER* nonsense mutation: unaffected individual (“homozygous wild-type”), obligatory carrier (“heterozygous carrier”), and an affected individual (“homozygous mutant”). **b** *SCAPER* proteomic abundance data generated using the Human Proteome Map (HPM) [32]. **c** Schematic demonstration of the two *SCAPER* variants: top panel shows the genomic location and exons; middle panel depicts the location of the various domains within *SCAPER*; lower panel highlights the location of the p.(L936*) variant, predicted to truncate both transcripts of *SCAPER* (demonstrated using Ingenuity® Variant Analysis™ isoforms viewed on gene views). **d**, **e** Western blot analysis of *SCAPER* protein in HeLa cells transfected

with either wild type (pCBF-FLAG-*SCAPER*), mutant FLAG-tagged *SCAPER* (pCBF-FLAG-mut*SCAPER*) or mock plasmid (pCBF-FLAG), stained using polyclonal anti-*SCAPER* (**d**) or anti-FLAG (**e**) antibodies. Mutant *SCAPER* protein was observed ~50 kDa smaller than the wild type. These findings were consistent when using either anti-FLAG or anti-*SCAPER* antibodies. **f** Although the transfection protocol was identical for all constructs, densitometry for wild-type *SCAPER* and its mutant counterpart (normalized to total lane protein) showed marked tenfold decrease in mutant protein level. The experiments (**d**, **e**) were repeated twice (biological replicates; ex.1, ex.2). Protein quantification data (**f**) integrate data from ex.1 and ex.2

heterozygotes for a possibly pathogenic mutation [41]. The *THSD4* and *C15ORF39* variants were also found at a heterozygous state, in 5.26% and 2.6%, respectively. No homozygotes for any of the variants were found in the

controls. It is noteworthy that the *THSD4* variant was the only one found outside the clan, in the larger tribe (found at the frequency of 0.625% in our in-house dataset, and validated using RFLP to exist at a heterozygous state apart from

the other variants, in three additional related individuals), further suggesting that it is a benign polymorphism.

The *SCAPER* mutation does not cause NMD

To test whether the *SCAPER* mutation causes nonsense-mediated mRNA decay (NMD), and as commercial anti-*SCAPER* antibodies failed to effectively detect endogenous *SCAPER* protein, we analyzed cDNA from fresh peripheral blood leukocytes of patient P2:IV1 and his parents (P2:III8 and P2:III9), testing quantitative expression levels of patients' RNA. Quantitative reverse transcription PCR (qRT-PCR) for *SCAPER* showed no significant change in transcript normalized concentration within affected individual's derived cDNA. Two heterozygotes tested showed values of 0.63 and 1.14 (calibrated to control cDNA), and the homozygous mutant showed a value of 0.63 (data not shown). Thus, despite the putative disruptive nature of the c.2806delC; p.(L936*) variant and the new premature stop codon, no significant NMD was noted.

SCAPER protein expression

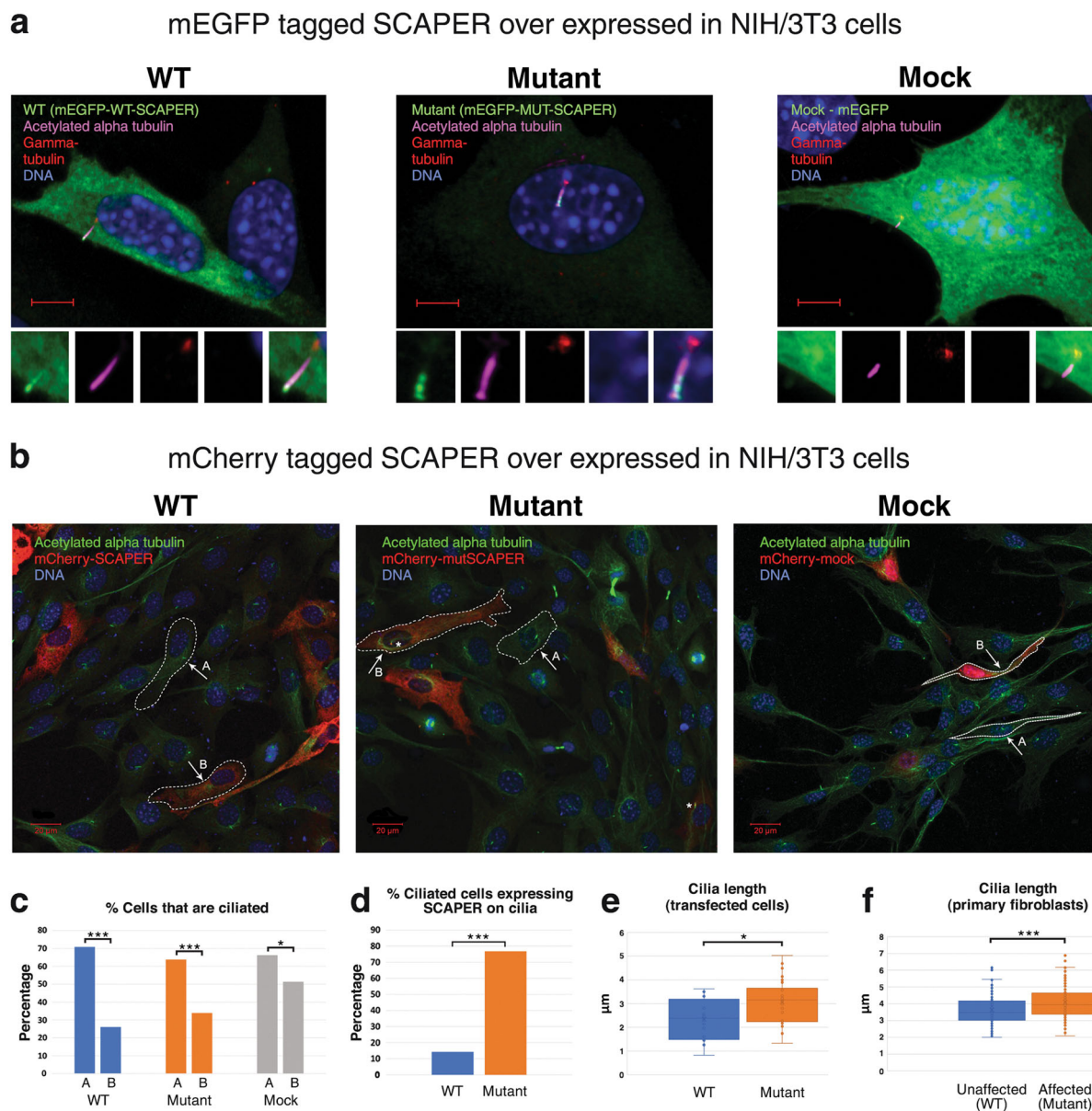
As the clinical phenotype of the affected individuals was very much reminiscent of that of ciliopathies such as BBS, we set out to test a possible role of *SCAPER* in primary cilia. Using two existing commercial anti-*SCAPER* antibodies, endogenous *SCAPER* protein could not be detected in untransfected (naïve) HeLa cells (Fig. 2d). Hence, the endogenous *SCAPER* expression level is below the detection level of the commercial antibody. Therefore, to study both WT and mutant *SCAPER*, we transfected with FLAG-tagged *SCAPER* constructs: WT pCBF-FLAG-*SCAPER*, mutant (truncated) pCBF-FLAG-mut*SCAPER* or a control mock plasmid, pCBF-FLAG. In HeLa cells transfected with the three constructs, the p.(L936*) mutant FLAG-tagged *SCAPER* (pCBF-FLAG-mut*SCAPER*) was observed ~50 kDa smaller than the WT, consistent with a C-terminally truncated protein (Fig. 2d, e). These findings were consistent when using either anti-FLAG (Fig. 2e) or polyclonal anti-*SCAPER* (Fig. 2d) antibodies. Although the transfection protocol was identical for all constructs, densitometry for WT *SCAPER* and its mutant counterpart (normalized to total lane protein) showed marked ten-fold decrease in mutant protein level ($n = 2$) (Fig. 2f), suggesting that the truncated protein is unstable.

To test possible expression of *SCAPER* in primary cilia, we went on to study protein localization in two cell lines: the primary cilia-expressing NIH/3T3 fibroblasts and the disease-relevant SH-SY5Y neuroblastoma cell lines, transfected with either WT or p.(L936*) truncated mutant *SCAPER* (Figs. 3a–e, 4). To ensure that the intracellular localization is not affected by the tag, experiments were

repeated with *SCAPER* constructs with either mEGFP or mCherry tags.

In NIH/3T3 cells fixed 16–24 h post transfection, the mEGFP/mCherry-WT-*SCAPER* protein was observed mostly diffusive in the cytoplasm of most cells (Fig. 3a, b). While most of those transfected cells did not demonstrate easily defined protruding cilium, naïve (un-transfected cells within the same randomly selected fields) did demonstrate high level of ciliation. Within this population of ciliated transfected cells, *SCAPER* could be found as a dense spot in and near the basal body or along the primary cilia and its tip (Fig. 3a, b). The truncated mEGFP/mCherry-MUT-*SCAPER* also showed mostly diffuse cytoplasmic pattern and similar percentage of ciliation (Fig. 3c); however, in contrast with the over-expressed WT protein, the mutant protein was constantly observed in the primary cilia (Fig. 3d), mostly at the tip of the cilia, distal from the basal body. Mock mEGFP/mCherry did not present any specific pattern of localization, with diffuse expression throughout the cytoplasm and the nucleus (Fig. 3a, b). Mock transfected cells also demonstrated reduced level of ciliation in comparison to the naïve (un-transfected cells) within same fields (Fig. 3b, c), but were never found localized on the primary cilia in our experiments. The intracellular localization phenotype above was seen mostly in cells with low expression levels of the fluorescently tagged proteins. In contrast, mostly aggregated fluorescent-tagged protein was seen in cells with high expression levels of both the transfected mEGFP and mCherry-tagged WT and mutant *SCAPER* plasmids at the time of fixation. We noticed fibrillar pattern seldom in some of the formalin fixed cells, more common in the mEGFP tagged WT/Mut- *SCAPER* (data not shown).

In an effort to study (cilia) dynamics, we went on to do live imaging of non-fixed cells in the first 8–24 h after transfection with WT or mutant mCherry or mEGFP fluorescent-tagged *SCAPER*. As seen in Fig. 4, at 12 h post-transfection, both WT and mutant *SCAPER* (yet not the mock transfection) were evident as a prominent fluorescently-tagged fibrillar structure. A dense spot or two close dense spots were seen in most cells, with possibly borderline thicker fibrillar structure with the mutant protein. Similar results were obtained with different cell lines (Fig. 4a, b). Co-localization of mCherry-tagged MUT *SCAPER* with another exogenous fluorescent-tagged protein, eGFP- α tubulin, suggested that the tubular structure is composed of microtubules (Fig. 4c, d). The cellular organization of both WT and mutant *SCAPER* in tubular structure was more prominent in the less ciliated and rapidly dividing SH-5YSY cells than in NIH/3T3 cells. Unfortunately, we could not follow ciliary or cell cycle dynamics, as most transfected cells rapidly progressed to apoptosis/necrosis, with no evident progress in cell cycle.



As SCAPER was evident at the tip of cilia, we investigated a possible effect of the SCAPER mutation on cilia length: as seen in Fig. 3e, NIH/3T3 cells transfected with mutant SCAPER had longer cilia than those transfected with WT SCAPER. This was further corroborated through scanning electron microscopy (SEM) of primary, non-transfected, skin fibroblasts of an affected individual versus a non-affected control: SEM of 6 cilia of an affected individual and of 6 cilia of a control demonstrated no structural differences. However, cilia length seemed longer in the mutants (supplementary figure 1). To quantify a possible difference in cilia length in naïve human mutant versus control fibroblasts, confocal microscopy was used to assess cilia length (see methods), testing a total of 232 cilia (119 wild type, 113 mutant). As seen in Fig. 3f, cilia in naïve

affected (homozygous mutant) human fibroblasts were significantly longer than those in the naïve control fibroblasts ($p = 0.00019$), in line with the findings in transfected NIH/3T3 cells.

Discussion

The affected individuals in our study presented with a combination of phenotypes characteristic of ciliopathies (with some overlap with BBS) [3, 5], including photoreceptor degeneration, obesity, intellectual disability, speech impediment, developmental delay and behavioral abnormalities, as well as phenotypes found in BBS at a lesser frequency, such as brachydactyly, ataxia, and

◀ **Fig. 3** SCAPER localization and ciliary phenotype in NIH/3T3 cells and cilia length in primary fibroblasts: **a** Exogenous SCAPER tagged with mEGFP localizes to the primary cilia: NIH/3T3 cells transfected with mEGFP-WT/MUT-SCAPER plasmids (over-expressing wild type or mutant p.(L936*) SCAPER, N'-tagged with mEGFP, shown in green), and stained for visualization of primary cilia and the basal body using anti acetylated alpha tubulin antibody (magenta) and anti-gamma tubulin antibody (red); logarithmic presentation ($\gamma = 2$), enabling identification of cilia axoneme (magenta) and basal body (red); DNA stained with DAPI (blue). Scale bar = 5 μm . Small panels, zooming on the primary cilia, demonstrate (left to right): mEGFP (green), Acetylated alpha tubulin (magenta), gamma tubulin (red), DAPI (blue) and overlay of all the above (ZEISS LSM880 microscope, 60 \times /1.4 objective). **b** Exogenous SCAPER tagged with mCherry localizes to the primary cilia as well: the experiments above were repeated with SCAPER N'-tagged with mCherry, with results similar to those in Fig. 3a. Acetylated alpha tubulin (ciliary axoneme) marked in green. As most cells were not dividing, low transfection rate and high percentage of ciliated cells was achieved in all experiments. Larger fields are presented: "A" and "B" mark the sub-populations of naïve (un-transfected) cells and transfected cells within each field studied, respectively. Asterisks mark primary cilia with SCAPER (in red) localized to it (ZEISS LSM880 microscope, 20 \times /0.8 objective). **c** Percentage of naïve (A) and transfected (B) cells that are ciliated: Lower percentage of ciliated cells was noticed in all experiments among transfected cells, compared to non-transfected cells. The difference was less marked with mock mCherry and mEGFP (66% of ciliated cells in the naïve sub-population; 51% of ciliated cells in the transfected cells; $n = 145$ and 72 , respectively; $p = 0.035$), as compared with overexpression of wild-type SCAPER (71% vs. 26%; $n = 792$ and 188 ; $p < 0.001$), and mutant SCAPER (64% vs. 34%, $n = 613$ and 165 , $p < 0.001$). **d** Percentage of ciliated transfected cells in which SCAPER localized to cilia: Within the sub-population of cells that were both transfected and ciliated, SCAPER could seldom be found localized to the primary cilia in cells over-expressing WT SCAPER (14%, $n = 49$), while the mutant protein was constantly observed in the primary cilia (77%, $n = 56$; $p < 0.001$). The mock transfectants did not demonstrate any specific localization. **e** Quantification of cilia length in transfected cells: WT cilia were shorter than the mutants; lengths (mean) were 2.34 μm and 3.07 μm , respectively ($n = 16$, $n = 30$, respectively; $p = 0.013$; only cells visualized with X60/1.2 objective were measured). **f** Quantification of cilia length in primary non-transfected skin fibroblasts of mutant (affected, patient P2:IV1) versus wild type (healthy control) individuals: WT cilia were shorter than the mutant cilia; lengths (mean) calculated were 3.62 μm and 4.09 μm , respectively (3 technical repeats, $n = 119$, $n = 113$, respectively; $p = 0.00019$; further details in Methods and in supplementary figure 1). All NIH/3T3 transfected cells were assayed 16–24 h post transfection

cataracts (Table 1 and S1 Table). Through homozygosity mapping and whole exome sequencing, we demonstrated that the disease is caused by a *SCAPER* truncation mutation.

SCAPER was previously associated with certain aspects of the studied phenotype: a single homozygous *SCAPER* mutation was implicated in causation of non-syndromic familial mental retardation in three children (age was unspecified) [38]. In a genome wide association study (GWAS), *SCAPER* was shown to have statistically significant association with low general cognitive ability [40]. Recently, in a large whole genome sequencing study of RP patients [37] a single individual was shown to have

compound heterozygous mutations in *SCAPER*. The patient was described as having multiple phenotypes, perhaps being syndromic (no further information was available). Moreover, a very recent study, conducted parallel to and unrelated to our study, demonstrated bi-allelic mutations in *SCAPER* as the cause for autosomal recessive RP with intellectual disability and attention deficit/hyperactivity disorder, in four patients of three unrelated families [39].

Although demonstrated before to endogenously exist within human and mouse cell-lines (using non-commercial antibody) [17], the endogenous *SCAPER* protein levels were un-demonstrable using commercial antibodies. We therefore transfected HeLa cells with plasmids expressing either the WT or the mutant protein conjugated to FLAG. The mutant transcript did not undergo significant NMD and the encoded protein was shown to be ~50 kD smaller than its WT counterpart.

Next, through transfection with mCherry-*SCAPER* and mEGFP-*SCAPER* plasmids in parallel to immunostaining with markers of primary cilia in NIH/3T3 fibroblasts, we demonstrated that both WT and mutant *SCAPER* localize to the primary cilia, mostly at their tip. While mutant *SCAPER* was persistently localized to the cilia, its WT counterpart was missing from the cilia in most ciliated cells. It should be noted that while most non-transfected cells were ciliated, cilia were significantly less evident in cells transfected with WT *SCAPER*, or to a lesser degree—in cells transfected with mutant *SCAPER*. As a similar effect (though to lesser degree) was seen with the mock transfection, this lower level of ciliation within transfected cells could be attributed at least in part to the transfection event itself (as it is more common in dividing, thus un-ciliated cells), to aggregation created or due to cellular toxicity. However, as the effect was most noticeable in WT *SCAPER* transfectants, the reduced ciliation in the *SCAPER*-transfected cells might be at least in part due to a change in cilia formation/preservation/resorption, or in cell-cycle progression dynamics, as *SCAPER* is known to affect cell cycle distribution; notably, Tsang et al. demonstrated that *SCAPER* over-expression results in M phase delay, and their data suggest that the delay may occur in the prophase stage of mitosis [17].

In cells with high levels of expression of either mutant or WT *SCAPER*, *SCAPER* was evident (localized) in microtubule-like, as well as cilia-like or basal body-like organelle. The same phenomenon was seen with both mCherry and mEGFP conjugates, and was even more evident in live cell imaging (12 h post-transfection) of non-fixated cells, and in SH-SY5Y cells. Co-expressing mutant *SCAPER* protein with fluorescently tagged alpha-tubulin (live imaging), revealed the microtubule-like bundles to be indeed microtubule structures, suggesting that *SCAPER* is a microtubule related protein. Our findings regarding expression of

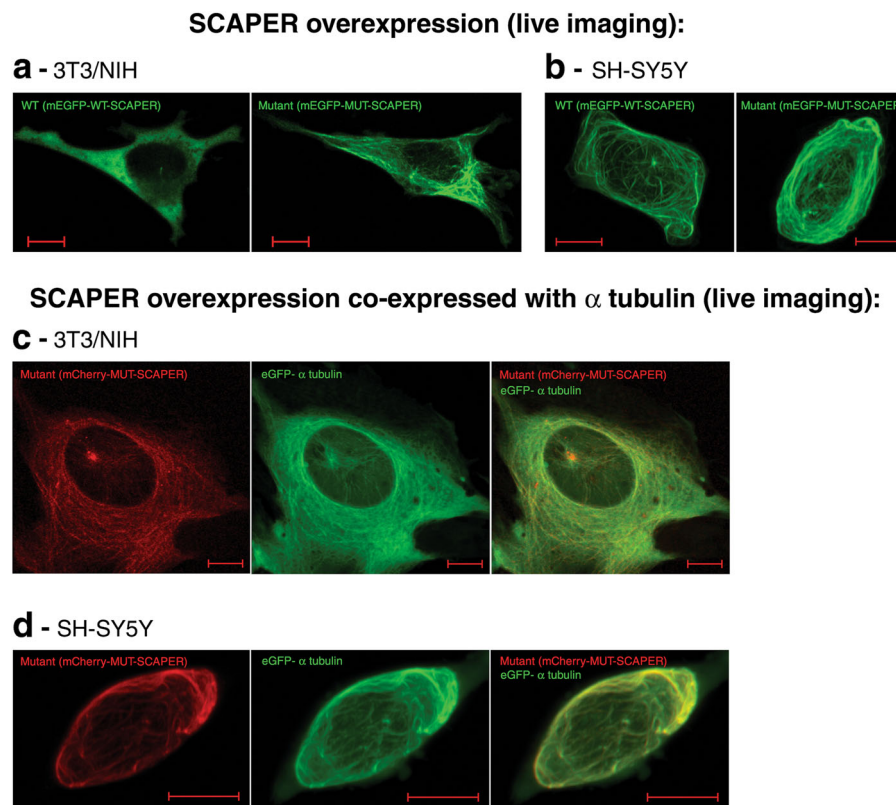


Fig. 4 Live-imaging of non-fixed cells over-expressing SCAPER, presenting tubular structure: **a, b** Overexpression of the N' mEGFP tagged SCAPER wild-type or mutant p.(L936*) truncated protein in NIH/3T3 cells (**a**) and SH-5YSY cells (**b**): diffuse and cilia-like or basal body-like organelle localization is evident, as well as a tubular structure for the mutant construct in both cell lines. **c, d** Co-localization studies showing that the tubular structure expressing SCAPER is indeed a tubulin structure: overexpression of the N'

mCherry-tagged SCAPER mutant p.(L936*) truncated protein in NIH/3T3 cells (**c**) and SH-5YSY cells (**d**), co-expressed and co-localized with eGFP tagged alpha-tubulin in live cells. Note: cells were visualized using ZEISS LSM880 microscope with a 40 \times /1.2 objective, in FastAiryScan mode, in 2 or 3 separate tracks, as described in the methods section. The scale bar equals 10 μ m. Cells were imaged 12 h post transfection

SCAPER are similar to those observed with overexpression of other microtubule-related proteins. Furthermore, the pattern of localization of SCAPER on microtubules and the cilia, especially their tip, resembles that of proteins regulating microtubule dynamics, such as KIF7 [42]. Moreover, studies of SCAPER's homolog in *D. melangoster*, SSP3, suggested that it is part of the centrosome proteome [35], functionally affecting microtubules during mitosis [43]; furthermore, the ortholog of SCAPER in *M. musculus* is part of the cilium proteome (both the cytoskeleton and photosensory-cilium) [36], further supporting our in-vitro observations. Overall, our data show that SCAPER has affinity to microtubules, mostly ciliary axoneme and the basal body.

Although we have demonstrated SCAPER expression in primary cilia in cell culture, and that the SCAPER mutation affects cilia length, it should be noted that overexpression of proteins in cells, and especially with a large tag that may alter protein folding, may lead to altered localization and does not always reflect the endogenous location. Thus, at

this point one cannot determine with full certainty that SCAPER is indeed a ciliary protein in *H. Sapiens*.

SCAPER has been previously shown to be specifically associated with the cyclin A/Cdk2 (CCNA2/CDK2) complex: in the absence of SCAPER, the CCNA2/CDK2 complex is almost nonexistent in the cytoplasm, while when SCAPER is over-expressed, the complex is abundant in the cytoplasm, suggesting that SCAPER plays a role in the complex's exiting the nucleus or remaining there [17, 18]. Outside the nucleus, the Cyclin A/CDK2 complex regulates centrosome activation, a function essential for the duplication/replication of the centrosome [17, 44]. In fact, the CCNA2/CDK2 complex is essential for centrosome duplication in somatic cells and controls nuclear mitotic events [44, 45].

Aside from its association with the CCNA2 / CDK2 complex, SCAPER was shown to complex also with MOZART1 [46], a protein necessary for the formation of the gamma tubulin ring [47], which forms the basis for the nucleation of the microtubules of the primary cilia [48]. As

SCAPER expression is known to be cell-cycle dependent, and was previously shown to affect cell-cycle progression in a timely manner, it may possess a different role and location during meiosis and mitosis. SCAPER expression peaks at late G1 and S phase [17, 18], overlapping the timing of ciliary resorption [49], comprises part of the cilia proteome and affects mitotic spindle assembly [35, 36, 43]. Put together with our demonstration that it is likely a ciliary protein, these facts suggest a role of SCAPER in ciliary dynamics, affecting microtubule-related mitotic progression. Notably, longer cilia were demonstrated both in human affected fibroblasts compared to controls, as well as in NIH/3T3 cells transfected with mutant versus wildtype SCAPER, implying a possible role of WT SCAPER specifically in restricting cilia elongation or enhancing cilia resorption.

Overall, we outline a human ciliopathy syndrome and demonstrate that it is caused by a mutation in SCAPER, affecting primary cilia. While we have shown that SCAPER is expressed in-vitro in primary cilia and that the ciliopathy-causing mutation affects this expression and cilia length, future studies are needed to elucidate possible roles of SCAPER in cell cycle progression and in primary cilia function and dynamics.

Acknowledgements The studies were funded by the Israeli Ministry of Health grant number 3-11799, awarded to OSB, and supported through the National Knowledge Center for Rare/Orphan Diseases sponsored by the Israel ministry of Science, Technology and Space. We thank Merav Saroussy-Levy for secretarial assistance and Dr. Uzi Hadad, of the Ilse Katz Institute for Nanoscale Science & Technology at BGU, for technical assistance.

Compliance with ethical standards

Conflict of interest The authors declare that they have no conflict of interest.

Publisher's note: Springer Nature remains neutral with regard to jurisdictional claims in published maps and institutional affiliations.

References

- Reiter JF, Leroux MR. Genes and molecular pathways underpinning ciliopathies. *Nat Rev Mol Cell Biol.* 2017;18:533–47.
- Plotnikova OVOV, ENEN Pugacheva. Golemis EAEA. Primary cilia and the cell cycle. *Methods Cell Biol.* 2009;94:137–60.
- Waters AM, Beales PL. Ciliopathies: an expanding disease spectrum. *Pediatr Nephrol.* 2011;26:1039–56.
- Zaghloul Na, Katsanis N. Science in medicine mechanistic insights into Bardet-Biedl syndrome, a model ciliopathy. *J Clin Invest.* 2009;119:428–37.
- Beales PL, Elcioglu N, Woolf AS, Parker D, Flintner FA. New criteria for improved diagnosis of Bardet-Biedl syndrome: results of a population survey. *J Med Genet.* 1999;36:437–46.
- Erickson RP, & Wynshaw-Boris AJ (Eds.). *Epstein's inborn errors of development.* Oxford University Press; 2016 <https://doi.org/10.1093/med/9780199934522.001.0001>.
- Heon E, Kim G, Qin S, et al. Mutations in C8ORF37 cause Bardet Biedl syndrome (BBS21). *Hum Mol Genet.* 2016;25:2283–94.
- Khan AO, Decker E, Bachmann N, Bolz HJ, Bergmann C. C8orf37 is mutated in Bardet-Biedl syndrome and constitutes a locus allelic to non-syndromic retinal dystrophies. *Ophthalmic Genet.* 2016;37:290–3.
- Lindstrand A, Frangakis S, Carvalho CMB, et al. Copy-number variation contributes to the mutational load of Bardet-Biedl syndrome. *Am J Hum Genet.* 2016;99:318–36.
- Markus B, Alshafee I, Birk OS. Deciphering the fine-structure of tribal admixture in the Bedouin population using genomic data. *Heredity.* 2014;112:182–9.
- Na'amnih W, Romano-Zelekha O, Kabaha A, et al. Prevalence of consanguineous marriages and associated factors among Israeli Bedouins. *J Community Genet.* 2014;5:395–8.
- Farag TI, TEEBI AS. Bardet-Biedl and Laurence-Moon syndromes in a mixed Arab population. *Clin Genet.* 1988;33:78–82.
- Yogev Y, Perez Y, Noyman I et al. Progressive hereditary spastic paraplegia caused by a homozygous KY mutation. *Eur J Hum Genet.* 2017. <https://doi.org/10.1038/ejhg.2017.85>.
- Seelow D, Schuelke M, Hildebrandt F, Nürnberg P. HomozygosityMapper—an interactive approach to homozygosity mapping. *Nucleic Acids Res.* 2009;37:593–9.
- Silberstein M, Weissbrod O, Otten L, et al. A system for exact and approximate genetic linkage analysis of SNP data in large pedigrees. *Bioinformatics.* 2013;29:197–205.
- Volodarsky M, Markus B, Cohen I, et al. A deletion mutation in TMEM38B associated with autosomal recessive osteogenesis imperfecta. *Hum Mutat.* 2013;34:582–6.
- Tsang WY, Wang L, Chen Z, Sánchez I, Dynlacht BD. SCAPER a novel cyclin A-interacting protein that regulates cell cycle progression. *J Cell Biol.* 2007;178:621–33.
- Tsang WY, Dynlacht BD. Double identity of SCAPER: a substrate and regulator of cyclin A/Cdk2. *Cell Cycle.* 2008;7:702–5.
- Goliand I, Nachmias D, Gershony O, Elia N. Inhibition of ESCRT-II-CHMP6 interactions impedes cytokinetic abscission and leads to cell death. *Mol Biol Cell.* 2014;25:3740–8.
- Vangipuram M, Ting D, Kim S, Diaz R, Schüle B. Skin punch biopsy explant culture for derivation of primary human fibroblasts. *J Vis Exp.* 2013. <https://doi.org/10.3791/3779>.
- Witteveen JS, Willemsen MH, Dombroski TCD, et al. Haploinsufficiency of MeCP2-interacting transcriptional co-repressor SIN3A causes mild intellectual disability by affecting the development of cortical integrity. *Nat Genet.* 2016;48:877–87.
- Mykytyn K, Braun T, Carmi R, et al. Identification of the gene that, when mutated, causes the human obesity syndrome BBS4. *Nat Genet.* 2001;28:188–91.
- ExAC Browser. <http://exac.broadinstitute.org/>. Accessed 8 Jan 2018.
- gnomAD browser. <http://gnomad.broadinstitute.org/>. Accessed 8 Jan 2018.
- Lek M, Karczewski KJ, Minikel EV, et al. Analysis of protein-coding genetic variation in 60,706 humans. *Nature.* 2016;536:285–91.
- Adzhubei IA, Schmidt S, Peshkin L, et al. A method and server for predicting damaging missense mutations. *Nat Methods.* 2010;7:248–9.
- Schwarz JM, Cooper DN, Schuelke M, Seelow D. MutationTaster2: mutation prediction for the deep-sequencing age. *Nat Methods.* 2014;11:361–2.
- AFC. <http://www.allelefrequencycommunity.org/>. Accessed 12 Mar 2017.
- Saito M, Kurokawa M, Oda M, et al. ADAMTSL6 β protein rescues fibrillin-1 microfibril disorder in a Marfan syndrome mouse model through the promotion of fibrillin-1 assembly. *J Biol Chem.* 2011;286:38602–13.

30. Repapi E, Sayers I, Wain LV, et al. Genome-wide association study identifies five loci associated with lung function. *Nat Genet.* 2010;42:36–44.
31. Wilhelm M, Schlegl J, Hahne H, et al. Mass-spectrometry-based draft of the human proteome. *Nature.* 2014;509:582–7.
32. Kim M-S, Pinto SM, Getnet D, et al. A draft map of the human proteome. *Nature.* 2014;509:575–81.
33. Human Proteome Map. <http://www.humanproteomemap.org/>. Accessed 8 Jan 2018.
34. Arnaiz O, Cohen J, Tassin AM, Koll F. Remodeling Cildb, a popular database for cilia and links for ciliopathies. *Cilia.* 2015. <https://doi.org/10.1186/2046-2530-4-S1-P21>.
35. Müller H, Schmidt D, Steinbrink S, et al. Proteomic and functional analysis of the mitotic *Drosophila* centrosome. *EMBO J.* 2010;29:3344–57.
36. Liu Q, Tan G, Levenkova N, et al. The proteome of the mouse photoreceptor sensory cilium complex. *Mol Cell Proteom.* 2007;6:1299–317.
37. Carss KJ, Arno G, Erwood M, et al. Comprehensive rare variant analysis via whole-genome sequencing to determine the molecular pathology of inherited retinal disease. *Am J Hum Genet.* 2017;100:75–90.
38. Najmabadi H, Hu H, Garshasbi M, et al. Deep sequencing reveals 50 novel genes for recessive cognitive disorders. *Nature.* 2011;478:57–63.
39. Tatour Y, Sanchez-Navarro I, Chervinsky E, et al. Mutations in SCAPER cause autosomal recessive retinitis pigmentosa with intellectual disability. *J Med Genet.* 2017;54:698–704.
40. Hill WD, Davies G, Liewald DC et al. Examining non-syndromic autosomal recessive intellectual disability (NS-ARID) genes for an enriched association with intelligence differences. *Intelligence* 2016;54:80–9.
41. Alkuraya FS. Discovery of mutations for Mendelian disorders. *Hum Genet.* 2016;135:615–23.
42. He M, Subramanian R, Bangs F, et al. The kinesin-4 protein Kif7 regulates mammalian Hedgehog signalling by organizing the cilium tip compartment. *Nat Cell Biol.* 2014;16:663–72.
43. Goshima G, Wollman R, Goodwin SS, et al. Genes required for mitotic spindle assembly in *drosophila* S2 cells. *Science (80-).* 2007;316:417–21.
44. De Boer L, Oakes V, Beamish H, et al. Cyclin A/cdk2 coordinates centrosomal and nuclear mitotic events. *Oncogene.* 2008;27:4261–8.
45. Meraldi P, Lukas J, Fry AM, Bartek J, Nigg EA. Centrosome duplication in mammalian somatic cells requires E2F and Cdk2-cyclin A. *Nat Cell Biol.* 1999;1:88–93.
46. Hein MY, Hubner NC, Poser I, et al. A human interactome in three quantitative dimensions organized by stoichiometries and abundances. *Cell.* 2015;163:712–23.
47. Masuda H, Mori R, Yukawa M, Toda T. Fission yeast MOZART1/Mzt1 is an essential -tubulin complex component required for complex recruitment to the microtubule organizing center, but not its assembly. *Mol Biol Cell.* 2013;24:2894–906.
48. Kollman JM, Merdes A, Mourey L, Agard DA. Microtubule nucleation by γ -tubulin complexes. *Nat Rev Mol Cell Biol.* 2011;12:709–21.
49. Sánchez I, Dynlacht BD. Cilium assembly and disassembly. *Nat Cell Biol.* 2016;18:711–7.